Molecular Simulations of Anhydrous $Na_6[Al_6Si_6O_{24}]$ Sodalite

Eric C. Moloy,*[,†,‡] Randall T. Cygan,[‡] François Bonhomme,[‡] David M. Teter,[‡] and Alexandra Navrotsky[†]

Thermochemistry Facility, Department of Chemical Engineering and Materials Science, University of California at Davis, Davis, California 95616-8779, and Geochemistry Department, Sandia National Laboratories, Albuquerque, New Mexico 87185-0750

Received November 26, 2003. Revised Manuscript Received February 19, 2004

An empirical energy force field, one that combines previously published force field parameters with a flexible SPC water model, is used to examine the structures and dynamical properties of the hydrosodalite family of zeolitic materials. In this paper, we present the results for $Na_6[Al_6Si_6O_{24}]$, one of two anhydrous end-members in this family. Experimentally derived unit cell volumes, T−O bond lengths, and T−O−T and O−T−O bond angles are used to validate the force field. Supplemental plane-wave pseudopotential density functional calculations fully support the potential-based models. Although sodalite materials usually possess $P\bar{4}3n$ symmetry, the direct modeling results from both simulation techniques employed in this study suggest the formation of volume-doubled *C*2/*c* supercells. The loss of symmetry is due to the presence of only six monovalent ions in the unit cell, rather than the usual eight. This result stands in partial agreement with recent simulation and experimental studies that report volume-doubled *Pcn*2 and orthorhombic supercell structures, respectively. More specifically, Le Bail profile and Rietveld refinements—when compared to the synchrotron-based XRD data from the recent experimental study—favor *P*2/*c* symmetry, a sub-group of *C*2/*c*. Le Bail profile agreement indices of $R_P = 6.18\%$ and $R_{WP} = 7.92\%$ for *P*2/*c* are lower than those reported for the orthorhombic cases, and Rietveld refinement indices of $R_P = 7.91\%$ and $R_{WP} = 10.50\%$ are lower than those reported for *Pcn2*. We further propose a new S6R ring structure that can be explained in terms of two crystallographically and energetically distinct oxygen sites. These structural and energetic results offer explicit evidence to support the hypothesis that "vacant ring avoidance" drives supercell formation. The new S6R structure leads to the formation of two enantiomeric β-cages, which, in turn, leads to the volume-doubled supercell. Finally, the periodic DFT calculations suggest that the sodium ions occupy the centers of the six-membered rings, in full agreement with the force field results. This arrangement, however, stands in contrast to the results of a recent DFT study, where a significant offset of the sodium ions out of the planes of the S6Rs is observed.

Introduction

Zeolites are nanoporous materials, formed from both natural and synthetic processes, characterized as open-framework, aluminosilicate structures comprised of corner-sharing tetrahedra (tectosilicates). The structures possess extraframework cations, as necessary, for charge balance from the incorporation of $[AlO_4]^{-1}$ tetrahedra. In accordance with Lowenstein's rule,[1] which states that there are no Al−O−Al bonding sequences, but rather Al−O−Si−O−Al, the greatest amount of aluminum that can be incorporated into an aluminosilicate structure is one with a Si/Al molar ratio of unity. Whereas the extraframework cations are usually hydrated to various extents, the role of water with respect to formation, structure, stability, and reactivity remains a largely open question. Although water is not an integral component of zeolitic frameworks, about two-thirds of the approximately 150 classified framework types[2] collapse upon complete, or even partial, dehydration. It has been found that some zeolitic frameworks cannot be completely dehydrated under conditions of either low pressure or high-temperature (while preserving the framework topology). Additionally, pure-silica zeolites (hydrophobic, and therefore water-free) are found to exist in only approximately twenty framework types.

Nitrate bearing cancrinite and sodalite have formed in the caustic chemical conditions of some high-level nuclear-waste treatment facilities.[3−5] These precipitated phases have fouled expensive process equipment, and

* To whom correspondence should be addressed. Tel: 530-753-2597. Fax: 530-752-9307. E-mail: ecmoloy@ucdavis.edu.
† University of California at Davis.
‡ Sandia National Laboratories.

(1) Loewenstein, W. *Am. Miner.* **1954**, *39*, 92−96.
(2) International Zeolite Association, 2004; www.iza.ethz.ch/IZA.
(3) Weber, C. Oak Ridge National Laboratory (UT-Batelle) Report; ORNL/TM-2001/109; Oak Ridge, TN, 2001.
(4) Bickmore, B. R.; Nagy, K. L.; Young, J. S.; Drexler, J. W. *Environ. Sci. Technol.* **2001**, *35* (22), 4481−4486.
(5) Jove-Colon, C. F.; Krumhansl, J. L.; Xu, H.; Navrotsky, A.; Nyman, M. (preparation).

10.1021/cm0352302 CCC: $27.50
Published on Web 05/08/2004

are thought to be the primary constituents of the resilient heels in the bottom of Savannah River storage tanks.[5] Approximately one million gallons of high-level nuclear-waste fluid may have leaked into the sediment of the U.S. Department of Energy (DOE) Hanford Site.[4] The role of these phases with respect to radionuclide (primarily ^{137}Cs) containment and diffusion remains an open and very important question, as only a small percentage of the total nuclear waste has been processed.[5]

Although a variety of experimental techniques are being used to examine this problem—including solubility experiments, calorimetric measurements, and NMR spectroscopy—literature data for these zeolitic systems are sparse. Atomistic modeling techniques, including molecular mechanics (MM), molecular dynamics (MD), and density functional theory (DFT), may therefore provide insightful information regarding these complex and unique systems. Subjects of interest include energies of hydration, the preferred sites/positions of water, the role of water on radionuclide diffusion, and the effect of stacking faults on radionuclide retention. Because of the complex nature of such an analysis, the modeling work is broken down into two components. Although the ultimate objective is to study nitrate bearing sodalite, some very interesting results have been obtained for the anhydrous end-member of nonbasic, anhydrous $Na_6[Al_6Si_6O_{24}]$ sodalite. Future papers will address the hydrated variants, $Na_6[Al_6Si_6O_{24}]\cdot(H_2O)_n$, and the $Na_8(NO_3)_2[Al_6Si_6O_{24}]\cdot(H_2O)_n$.

Sodalite Structure

Sodalite is most technically classified as a feldspathoid. However, because this family of materials utilizes a primary building unit (PBU) common to many zeolitic frameworks—the β-cage—sodalite is also classified as a zeolite. Natural sodalite ($Na_8Cl_2[Al_6Si_6O_{24}]$) is a relatively abundant mineral that can also be synthesized in the laboratory, along with many structural variants. The general structural formula can be written as

$$M_m^{q+}X_x^{r-}[Si_{12-n}Al_nO_{24}](H_2O)_{0-8} \qquad (1)$$

where $qm - rx = n$, and $n \leq 6$. An equation describing the hydrosodalite family can be written as $(Na_{6+x}(OH)_x$-$[Si_6Al_6O_{24}](H2O)_{(8-2x)-0}$, where $0 \leq x \leq 2$. For simplicity, the $[Al_6Si_6O_{24}]$ framework is hereafter designated by [SOD][2]. Formally, every silicon atom carries a charge of 4^+ and every oxygen carries a charge of 2^-. Because oxygen atoms "bridge" two separate tetrahedra, each tetrahedron is charge neutral. The incorporation of aluminum, however, with a formal charge of 3^+, introduces a charge of 1^- to the framework for every AlO_4 tetrahedron. For a sodalite material with a Si/Al ratio of unity, the framework formula $[Al_6Si_6O_{24}]$ possesses a formal charge of 6^-. This charge must be compensated by extraframework cations (M^{q+}), which are oftentimes associated with extraframework anions (X^{r-}). Notice that the *sum* of the extraframework ion charges (cations *plus* anions) must equal n. Monovalent alkali metals (Na^+, Li^+, and K^+) and Ca^{2+} are common cations in natural systems, and some of the monovalent halogens (Cl^-, Br^-, and I^-) are common anions.[6,7] However, a large variety of more complex anionic species can occupy the interiors of the β-cages, including $B(OH)_4^-$, ClO_4^{2-}, CO_3^{2-}, HCO_2^-, MoO_4^{2-}, MnO_4^-, NO_3^-, SCN^-, WO_4^-, CrO_4^{2-}, and SO_4^{2-}.[8-11] Finally, a high degree of substitution can occur on the tetrahedral (T) sites: Ge^{4+}, Ga^{3+}, P^{3+}, B^{3+}, and even Be^{2+} can be incorporated into the framework T-sites.[12,13]

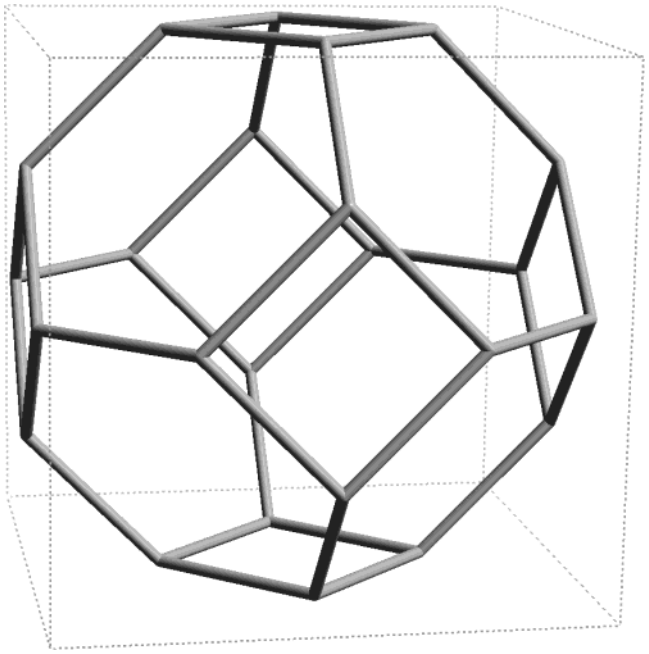

Figure 1. Unit cell of sodalite contains one fully constructed β-cage (idealized pure-silica structure, O atoms removed, perspective view). Every corner contains $^1/_8$ of a β-cage, however, so the volume of the unit cell is equivalent to the volume of two β-cages [ref 2].

The PBU of the sodalite framework is the β-cage, a very symmetrical cage constructed from six single 4-rings (S4Rs, four T-sites (T = Si, Al), and four O-sites) and eight S6Rs (Figure 1). The β-cage is also the PBU for a variety of other zeolitic frameworks[2] (AST, EMT, FAU, FRA, LTA, LTN, TSC), and knowledge about its fundamental properties may then be applicable to the more complex framework types. There is no characteristic channel system in [SOD], and the framework is characterized by "apertures" of S6Rs[2]. The β-cage can be thought of as a truncated cube: the six S4Rs are situated in the center position of each of the six sides of the cube, and the eight S6Rs are formed by "chopping" off small tetrahedra from each of the eight corners of the cube. Each β-cage is connected to eight other β-cages by sharing one of the eight S6Rs. This arrangement forms a BCC network of cages (Figure 2).

The idealized cubic unit cell is isometric and defined by the positions of 12 T-sites and 24 O-sites. The 12 T-sites result from four sites (with $^1/_2$ occupancy) in each of the six faces of the cubic unit cell. Twelve of the 24

(6) Mead, P. J.; Weller, M. T. *Zeolites* **1995**, *15* (6), 561−568.
(7) Nielsen, N. C., et al. *Zeolites* **1991**, *11* (6), 622−632.
(8) Fechtelkord, M. *Solid State Nucl. Magn. Reson.* **2000**, *18* (1−4), 70−88.
(9) Brenchley, M. E.; Weller, M. T. *Zeolites* **1994**, *14* (8), 682−686.
(10) Engelhardt, G., et al. *Solid State Nucl. Magn. Reson.* **1992**, *1* (3), 127−135.
(11) Park, H.; Englezos, P. *Ind. Eng. Chem. Res.* **1999**, *38* (12), 4959−4965.
(12) Weller, M. T., et al. *Stud. Surf. Sci. Catal.* **1997**, *105* (pt. A−C), 455−462.
(13) Jelinek, R.; Stein, A.; Ozin, G. A. *J. Am. Chem. Soc.* **1993**, *115*, 2390−2396.

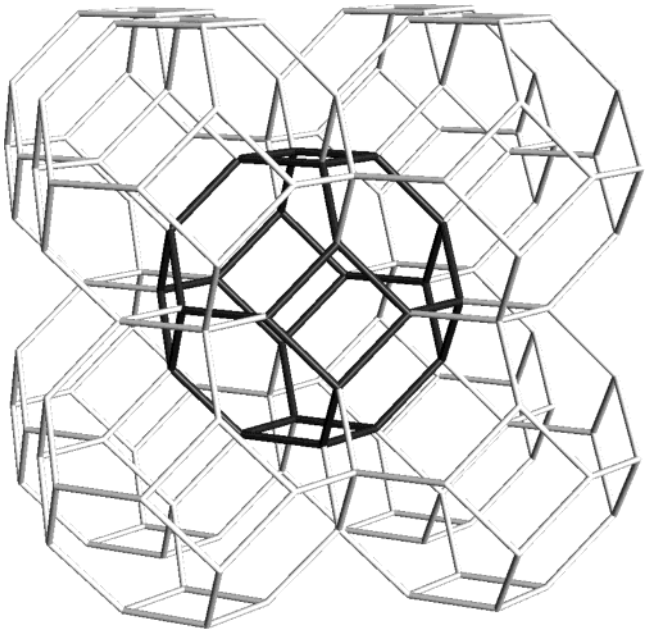

Figure 2. Sodalite framework (idealized pure-silica structure, O atoms removed, perspective view); any single β-cage (darkened) is surrounded by eight, octahedrally coordinated β-cages (by sharing the eight S6Rs). The framework can be thought of as a BCC arrangement of β-cages.

O-sites are completely contained within the unit cell, and the remaining 12 are located in the six faces of the unit cell, fully analogous to the T-site accounting. Although the unit cell contains one fully constructed β-cage, the total volume of the unit cell is equivalent to that of two β-cages: the central β-cage and eight partial cages (with $^1/_8$th cage volumes) in the corners that are shared with eight neighbor β−cages.

Sodium Distributions. Whereas most sodalite materials contain eight monovalent cation (M^+) and two monovalent anion species (X^-), the so-called "class A" sodalites, this study examines a particularly unique sodalite material—$Na_6[SOD]\cdot(H_2O)_n$. First reported as a "sodium poor"' sodalite in 1947 by Borchert and Keidel,[14] the presence of only six extraframework cations invokes unique unit cell distortions and asymmetric ring configurations for which considerable adsorption and exchange properties have been reported.[15]

The six extraframework Na^+ ions migrate close to the centers of the S6Rs in anhydrous sodalite. It turns out that there are three unique ways to distribute six Na^+ ions on the eight-point cubic array defined by the centers of the eight S6Rs. These eight T-sites fall on the 8*e* orbit of the $P\bar{4}3n$ space group. The three configurations are best described by the locations of the two vacant T-sites, which can lie along an edge (E), a face diagonal (FD), or a body diagonal (BD) of the cube defined by the 8*e* orbit. This paper denotes the three configurations using the nomenclature $Na_6[SOD]\cdot(H_2O)_n$ [X], where $n = 0-8$ and X = E, FD, or BD (Figure 3). The [E], [FD], and [BD] configurations are thought to drive orthorhombic, monoclinic, and rhombohedral distortions, respectively.[16]

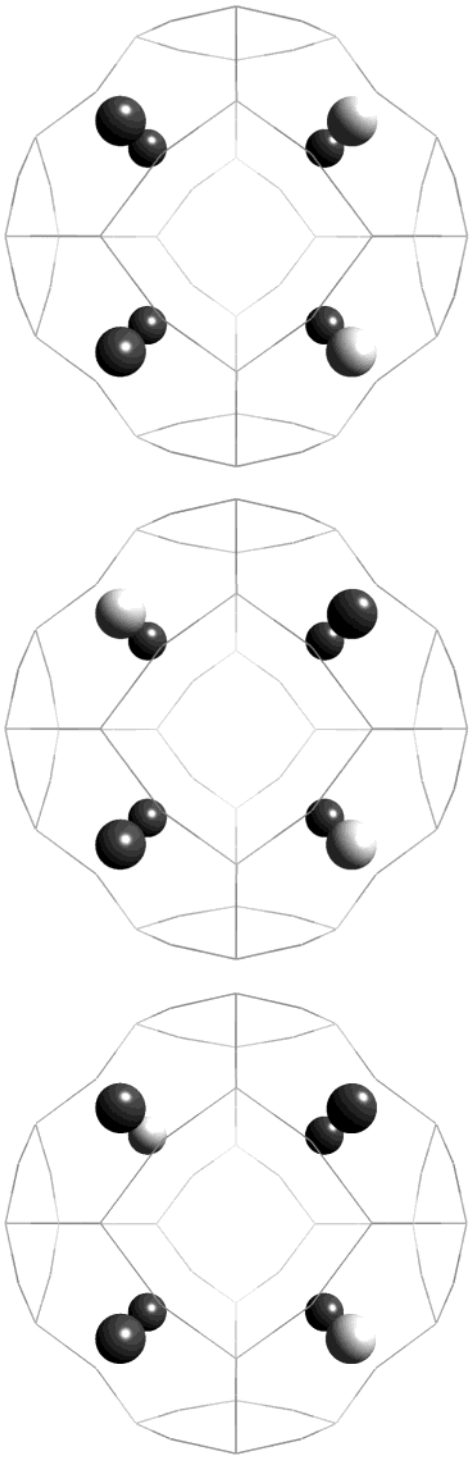

Figure 3. Three sodium arrangements in $Na_6[SOD]$ (idealized aluminosilicate structure, perspective views): the six dark-colored balls represent Na^+ ions, and the two light- colored balls represent vacant T-sites. The six Na^+ ions and the two vacancies are distributed on the *e* sublattice of space group $P\bar{4}3n$, for which there are eight lattice sites. The three configurations—designated in this report as (a) [E], (b) [FD], and (c) [BD]—refer to "edge", "face diagonal", and "body diagonal", and describe the locations of the two vacant T-sites on the cubic arrangement of the eight *e* lattice sites.

Ring Structures. There are three basic ring types in $Na_6[SOD]$: vacant S4Rs, vacant S6Rs (a S6R that

(14) Borchert, W.; Keidel, J. *Heidelb. Beitr. Miner. Petrog.* **1947**, *1*, 2−16.

(15) Felsche, J.; Luger, S.; Fischer, P. *Acta Crystallogr., Sect. C: Cryst. Struct. Commun.* **1987**, *C43* (5), 809−811.

(16) Shannon, S. R., et al. *J. Chem. Phys.* **2000**, *113* (22), 10215−10225.

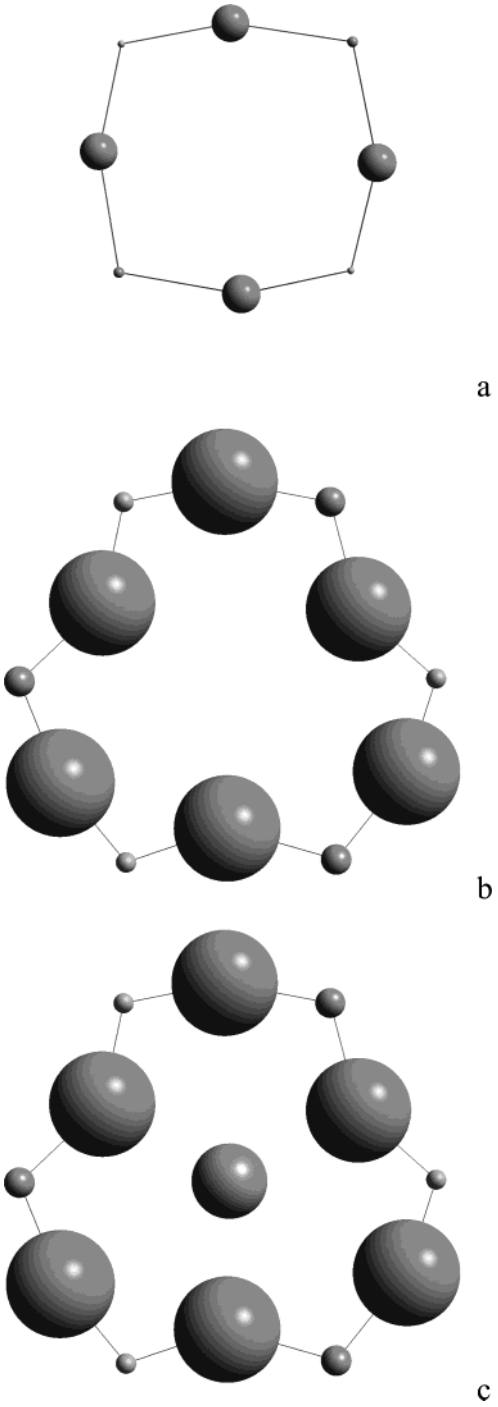

Figure 4. Three ring types in Na_6[SOD] [BD]: (a) S4R, (b) ^{V}S6R, and (c) ^{O}S6R (idealized structures, perspective views).

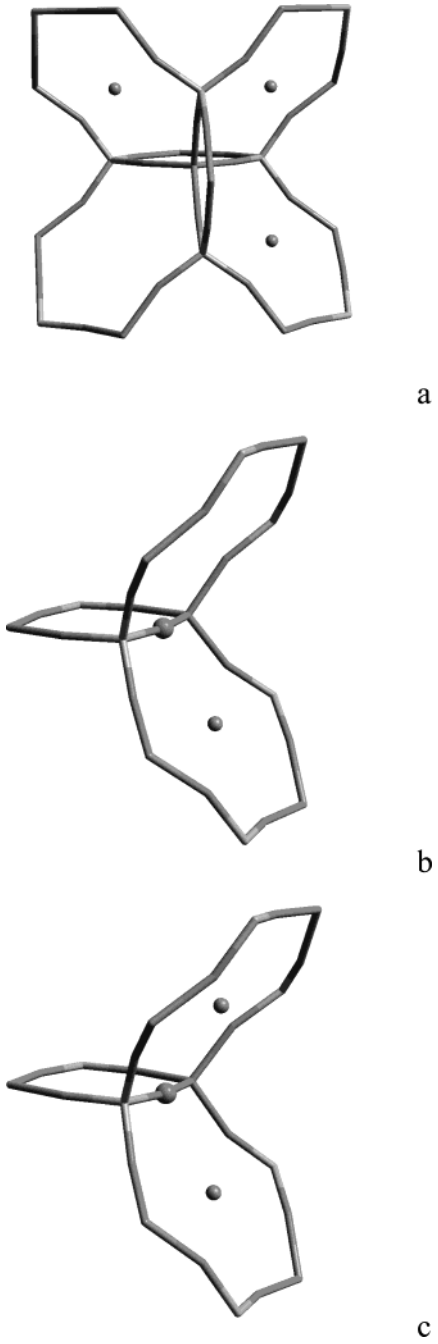

Figure 5. One T-site and two crystallographically unique oxygen sites in Na_6[SOD] [BD] (perspective views). (a) Every T-site is part of two S4Rs and four S6Rs. Every O atom is part of one S4R and two S6Rs: (b) Type ^{I}O involves one S6R−O and one S6R−V, and (c) Type ^{II}O involves two S6R−Os. The SOD [BD] structure contains equal numbers of ^{I}O and ^{II}O atoms.

does not contain a Na^+ ion), and occupied S6Rs (a S6R that does contain a Na^+ ion). The vacant/occupied S6Rs are designated by ^{V}S6R and ^{O}S6R. The S4R is never occupied, and does not require special nomenclature (Figure 4). A previous study[17] suggests that there are two unique ring environments associated with each of the three ring types. In contrast, the present study concludes that there is only one ring environment for each of the three basic ring types. Both simulation techniques (MM and DFT) employed in this study support this result. The disagreement stems from the different final models that result in the two respective studies. Because this is not an issue with respect to the results presented here, further elaboration is not warranted.

T-site loop configurations are important, standard ways by which to characterize zeolitic frameworks. Aside from the obvious chemical differences that exist between silicon and aluminum, every T-site in the sodalite framework is topologically equivalent with respect to loop configuration. Each T-site is an integral component of six separate and distinct rings: two S4Rs, one ^{V}S6R, and three ^{O}S6Rs (Figure 5 (a)). Although this

(17) Shannon, S. R.; Metiu, H. *J. Phys. Chem. B* **2001**, *105* (18), 3813−3822.

Table 1. Interatomic Potentials for the Various Chemical Species Associated with Na_6[SOD] (Rounded)

FF Species	charge (e)	σ (nm)	ϵ (kJ/mol)	ϵ (kcal/mol)	ref
zeolitic Si	+2.4	8.186	4.801×10^{-9}	1.147×10^{-9}	32
zeolitic Al	+1.4	0.831	$1.074 \times 10^{+4}$	2.565×10^{-3}	32
zeolitic O	−1.2	12.654	9.650×10^{-8}	2.305×10^{-8}	32
Na	+1.0	2.638	5.443×10^{-1}	1.300×10^{-1}	31

sort of analysis is not usually applied to the O-sites, it can be shown that each O-site is part of three distinct rings: one S4R and two S6Rs. A more significant distinction between O-sites, however, can be discerned: in $Na_6[Al_6Si_6O_{24}]$ one O-site will be part of *one* ^{V}S6R, *one* ^{O}S6R, and one S4R, while a second O-site will be part of *two* ^{O}S6Rs (no ^{V}S6R) and one S4R. It can be shown further that there are equal numbers of the two structurally distinct O-sites in Na_6[SOD] [BD], referred to hereafter as Type I (^{I}O) and Type II (^{II}O) oxygen sites (Figure 5 (b and c)). This issue will become more important when new ring structures are proposed for Na_6[SOD] [BD]. Finally, every S4R can be shown to have two ^{I}O and two ^{II}O-sites, every ^{V}S6R has six ^{I}O-sites, and every ^{O}S6R has two ^{I}O and four ^{II}O-sites.

Methodologies

Although a variety of zeolitic force fields have been developed to date,[18−28] few have been developed exclusively for hydrated zeolitic systems. In particular, it is important that the force field ultimately incorporates an accurate potential for water that is compatible with both the extraframework cations and all framework species—Si, Al, and O. The present simulations of anhydrous sodalite do not require a water potential; nonetheless, our choice of potential parameters requires compatibility for later simulations of the hydrated phase. Therefore, the flexible simple point charge (SPC) water potential was chosen[29] with the addition of the flexible parameters from ref 30, thereby allowing full flexibility of the H_2O molecule. The Na^+ ion potential was obtained from Smith and Dang[31] and is fully compatible with the SPC water model. Zeolitic aluminum, silicon, and oxygen potentials were obtained from the CVFF AUG IONIC 400 1.01 force field in Cerius^2,[32] which was originally derived as a nonbonded force field based on Columbic interactions and Lennard−Jones potentials. A complete list of the interatomic potentials can be found in Table 1. All atomistic simulations were performed using an SGI Octane or O^2 Unix workstation running Cerius^2 MS (version 4.2).[32] The OFF simulation engine was used in conjunction with the energy force field developed for the study of Na_6[SOD]·$(H_2O)_n$ in this paper.

Molecular Mechanics. The procedure by which a structural model is optimized has a profound and oftentimes unique impact upon the final, energy-minimized structure (i.e., the result is path-dependent). In this case, the two primary structural elements—the six Na^+ ions and the $[SOD]^{6-}$ framework—suggest that the energy minimizations can be conducted as one-step or two-step procedures. The one-step procedure introduces six Na^+ ions, arranged in one of the three configurations just discussed, into the unit cell, and then the entire system is energy-minimized under *P*1 symmetry. The two-step approach first minimizes the sodium-free, aluminosilicate $[SOD]^{6-}$ framework by using an electrostatic mean-field approximation to compensate for the net 6^- charge that results from the six aluminum framework cations. This minimization can then be performed enforcing either $P\bar{4}3n$ or *P*1 symmetry. After this initial minimization, the six Na^+ ions are loaded into the unit cell, and the system is minimized a second time using *P*1 symmetry. Three basic procedures are therefore possible, referred to in this report as *P*1, $P\bar{4}3n$−*P1*, and *P1*−*P1*. Finally, to test the effect of the initial placement of the Na^+ ions, Na^+ ions were placed in one of two initial positions: (a) near the center of the unit cell (3/8 3/8 3/8 with symmetry operations), and (b) in the faces of the respective S6Rs (1/4 1/4 1/4 with symmetry operations).

It should be noted that while the full relaxation of *P*1 symmetry would always be the desired procedure, *P*1 symmetry is necessarily required whenever six Na+ ions are in the system. An ordered distribution of the six sodium ions cannot be achieved in the $P\bar{4}3n$ space group. In order for Felsche and Luger[33] to obtain the $P\bar{4}3n$ structural model, for example, 75% occupancy of the 8*e* sites had to be incorporated.

To help ensure that the lowest possible lattice energies are obtained (models can become trapped in local energy minima during conformational energy searching), a unique, two-step relaxation technique called constrained constant pressure−constant pressure (CCP−CP) was developed. The first step is a CCP minimization that holds cell parameters α, β, and γ fixed, but allows *a*, *b*, and *c* to vary freely. The second step is a CP minimization that allows all six lattice parameters to vary freely. As discussed below, the two relaxation constraints (CCP−CP and CP) *can* produce different final structures. The differences can be very subtle yet significant: the lattice energies can *appear* to be numerically equivalent (to the precision reported by the software), but some structural features may differ slightly (bond lengths, bond angles, etc).

DFT Simulation. A second simulation approach was used to optimize the atomic coordinates of sodalite by minimizing the electronic energy of the zeolitic structure. These quantum calculations were conducted using an SGI Onyx II four-processor Unix workstation. This approach was carried out by a DFT method using the VASP code developed at the Institut fur Theoretische Physik of the Technische Universität Wien.[34−37] The quantum mechanical modeling of sodalite is a computationally demanding task. The problems of deep pseudopotentials required to accurately model the oxygen ion, combined with the low symmetry and large unit cell, would have made these calculations intractable until recently.

The electronic degrees of freedom were minimized using a residual minimization method direct inversion in the iterative subspace (RMM-DIIS) algorithm.[38,39] The VASP program

(18) Hill, J. R.; Sauer, J. *J. Phys. Chem.* **1995**, *99* (23), 9536−9550.
(19) Blake, N. P.; Weakliem, P. C.; Metiu, H. *J. Phys. Chem. B* **1998**, *102* (1), 67−74.
(20) de vos Burchart, E. V.; Van Bekkum, H.; Van de Graaf, B. *Zeolites* **1992**, *12* (2), 183−189.
(21) Jaramillo, E.; Auerbach, S. M. *J. Phys. Chem. B* **1999**, 9589−9594.
(22) Ricchiardi, G.; de Man, A.; Sauer, J. *Phys. Chem. Chem. Phys.* **2000**, *2* (10), 2195−2204.
(23) Faux, D. A.; Smith, W.; Forester, T. R. *Jo. Phys. Chem. B* **1997**, *101* (10), 1762−1768.
(24) Titiloye, J. O.; Parker, S. C.; Stone, F. S.; Catlow, C. R. A. *J. Phys. Chem.* **1991**, *95* (10), 4038−4044.
(25) Jackson, R. A.; Catlow, C. R. A. *Mol. Sim.* **1988**, *1*, 207−224.
(26) Sanders, M. J.; Leslie, M.; Catlow, C. R. A. *J. Chem. Soc., Chem. Commun.* **1984**, 1271−1273.
(27) Ermoshin, V. A.; Smirnov, K. S.; Bougeard, D. *Chem. Phys.* **1996**, *202* (1), 53−61.
(28) Ermoshin, V. A.; Smirnov, K. S.; Bougeard, D. *Chem. Phys.* **1996**, *209* (1), 41−51.
(29) Berendsen, H. J. C., et al. *Jerusalem Symp. Quantum Chem. Biochem.* **1981**, *14*, 331−42.
(30) Teleman, O.; Jonsson, B.; Engstrom, S. *Mol. Phys.* **1987**, *60* (1), 193−203.
(31) Smith, D. E.; Dang, L. X. *J. Chem. Phys.* **1994**, *100* (5), 3757−3766.
(32) Accelrys, 2004; www.accelrys.com.
(33) Felsche, J.; Luger, S. *J. Phys. Chem.* **1986**, *90* (8), 731−736.
(34) Kresse, G.; Furthmulle, J. *Comput. Mater. Sci.* **1996**, *6* (1), 15−50.
(35) Kresse, G.; Hafner, J. *Phys. Rev. B: Condens. Matter* **1993**, *47* (1), 558−561.
(36) Kresse, G.; Hafner, J. *Phys. Rev. B: Condens. Matter* **1994**, *49* (20), 14251−14269.
(37) Kresse, G.; Furthmuller, J. *Phys. Rev. B: Condens. Matter* **1996**, *54* (16), 11169−11186.
(38) Pulay, P. *Chem. Phys. Lett.* **1980**, *73* (2), 393−398.
(39) Wood, D. M.; Zunger, A. *J. Phys. A: Math. Gen.* **1985**, *18* (9), 1343−1359.

Table 2. Energy Differences between the Na_6[SOD] [E], [FD], and [BD] Configurations[a]

minimization method	ΔE (E-BD) eV/Na_6−SOD	ΔE (FD-BD) eV/Na_6−SOD	ΔE (E-BD) (kJ/mol-TO_2)	ΔE (FD-BD) (kJ/mol-TO_2)	ΔE (ratio)	ref
GGA-DFT	0.154	0.080	1.24	0.64	1.93	16
BWM	0.595	0.241	4.78	1.94	2.47	19
Shell	0.365	0.155	2.93	1.25	2.35	25, 26
MM EM			5.83	3.59	1.62	this study

[a] The force-field-based values from this study are reported with those from three other simulation studies.

derived the electronic charge density of anhydrous Na_6[SOD] using a density functional framework[40,41] within the local density approximation (LDA) electron exchange and correlation. The exchange correlation term of the total energy is the Perdew and Zunger parametrization[42] of the Ceperley and Alder data.[43] The electronic wave functions were expanded in a plane wave basis set with periodic boundary conditions. Vanderbilt ultra-soft pseudopotentials[44] were used for the oxygen ions with the $2s^2$ and $2p^4$ electrons being treated as valence electrons. Norm-conserving pseudopotentials was used for the aluminum (3s2, 3p1) sodium (3p1), and silicon (3s2, 3p2) ions. A kinetic energy cutoff of 495 *e*V was applied and a [222] MP grid was used for the Brillouin zone integration.

Results and Discussion

As noted previously, there is significant literature regarding sodalites in general, both empirical and simulation, but reports that consider Na_6[SOD] are sparse. Most recently, Campbell et al.,[45] using variable temperature synchrotron X-ray powder diffraction, suggested that Na_6[SOD] forms an orthorhombic or "pseudo-tetragonal" supercell. Shannon et al.,[16] using both classical force field energy minimization and DFT methods, report a similar result. Felsche and Luger, writing at least five articles in the mid-1980s, have probably contributed the most toward our understanding of Na_6[SOD]·$(H_2O)_n$.[15,33,46,47] In the end, two independent, experimental studies[33,45] were chosen by which to validate the simulation results.

Before proceeding, a few comments regarding the Shannon et al.[16] paper are warranted. Table 10 of that paper presents the fractional coordinates for their C_{24} orthorhombic supercell. The paper indicates that the symmetry of C_{24} possesses a *Pnc*2 space group. Personal communications with the authors concluded that the fractional coordinates presented in Table 10 are incorrect. Using corrected fractional coordinates, the symmetry of the unit cell was found to be *Pcn2*. This distinction is significant because *Pcn2* satisfies the "vacant ring avoidance" (i.e., no two ^{V}S6Rs sharing sides) principle while *Pnc*2 does not. We therefore conclude that the C_{24} structure is correctly referred to as *Pcn2*.

Configurational Energetics. As discussed previously, the six Na^+ ions can be distributed in one of three unique configurations on the 8*e* sublattice of the $P\bar{4}3n$ space group. Previous studies[16,17] have discussed these configurations, and consistent conclusions about the trend in energetics have been reached, including the results of this study (Table 2): $E_{BD} < E_{FD} < E_E$. Although the magnitudes of the relative energies ($\Delta E_E - \Delta E_{BD}$ and $\Delta E_{FD} - \Delta E_{BD}$) vary from study to study (1.24−5.83 and 0.64−3.59 kJ/mol-TO_2, respectively), the ΔE *ratios* ($\Delta E_{E-BD}/\Delta E_{FD-BD}$) exhibit more consistent behavior, ranging between 1.62 and 2.47. The observed energy differences can be attributed, at least in some part, to configurational entropy: the [BD] configuration has the greatest entropy and the lowest energy, and the [E] configuration has the lowest entropy and the highest lattice energy. Shannon et al.[16] suggest that "vacant ring avoidance" is the driving force for supercell formation, an interesting issue that will be discussed shortly. Because the [BD] configuration has the lowest lattice energy, all subsequent [SOD] simulations employ this configuration.

Minimization Procedures. Two energy-minimization techniques—one using Na_6[SOD] and a second using first $[SOD]^{6-}$ followed by Na_6[SOD]—along with two relaxation constraints (CCP−CP and CP), and two Na^+ ion starting positions, produce a total of twenty possible procedures by which to minimize Na_6[SOD]. For clarity, CCP−CP is actually a two-step minimization, but we refer to it as a single step. The initial placements of the Na^+ ions did not affect the final structures in any way, reducing the number of procedures to ten, from which three unique structures were produced. However, we will discuss the results of four procedures. The fourth case helps illustrate how important the minimization pathway can be toward the final, optimized structure. Two DFT simulations were also conducted to help elucidate the sodalite structure. Procedures, techniques, unit cell volumes (UCVs), and supercell space groups for the six procedures are listed in Table 3.

To illustrate how different symmetry constraints can significantly effect the minimized structures, consider the MM4 and MM3 procedures (Tables 1 and 3). Both are two-step procedures employing *P*1/CP symmetry/constraints during the secondary Na_6[SOD] minimization. However, MM4 enforces $P\bar{4}3n$ symmetry during the initial $[SOD]^{6-}$ minimization while MM3 employs *P*1 symmetry. The UCVs after the first minimization differ by 16.5 Å^3 (831.6 and 815.1 Å^3, respectively). After the subsequent Na_6[SOD] minimization, the UCVs differ by 11.7 Å^3, the lattice energies differ by 2.4 kJ/mol-TO_2, and the supercell symmetries are different. Thus, structural differences that existed between the two procedures after the first minimization carried over into the second step.

To illustrate the impact of different relaxation constraints, compare the results of the MM2 and MM3 procedures. Both are two-step procedures that employ

(40) Hohenberg, P.; Kohn, W. *Phys. Rev.* **1964**, *B136*, 864−871.
(41) Kohn, W.; Sham, L. J. *Phys. Rev.* **1965**, *140*, 1133−1138.
(42) Perdew, J. P.; Zunger, A. *Phys. Rev. B: Condens. Matter* **1981**, *23* (10), 5048−5079.
(43) Ceperley, D. M.; Alder, B. J. *Phys. Rev. Lett.* **1980**, *45* (7), 566−569.
(44) Vanderbilt, D. *Phys. Rev. B: Condens. Matter* **1990**, *41* (11), 7892−7895.
(45) Campbell, B. J., et al. *J. Chem. Phys.* **2000**, *113* (22), 10226−10239.
(46) Felsche, J.; Luger, S. *Thermochim. Acta* **1987**, *118*, 35−55.
(47) Felsche, J.; Luger, S.; Baerlocher, C. *Zeolites* **1986**, *6* (5), 367−372.

Table 3. Six Unique Na_6[SOD] Models Examined in This Study

procedure[a]	structure minimized	technique (no. of steps)	symmetry	relaxation constraint	initial UCV (Å^3)	final UCV (Å^3)	supercell symmetry	ΔE (kJ/mol-$Na_{0.5}TO_2$)
MM1	Na_6[SOD]	1	*P*1	CCP−CP	702.6	754.7	*R*3*c* (No. 161)	4.5
MM2	[SOD]	2	*P*1	CCP−CP	702.6	811.2		
	Na_6[SOD]		*P*1	CP	811.2	759.7	$\bar{R}$3 (No. 148)	0.0
MM3	[SOD]	2	*P*1	CP	702.6	815.1		
	Na_6[SOD]		*P*1	CP	815.1	748.0	*C*2/*c* (No. 15)	2.4
MM4	[SOD]	2	$\bar{P}$43*n*	CP	820.7	831.6		
	Na_6[SOD]		*P*1	CP	831.6	759.7	$\bar{R}$3 (No. 148)	0.0
GGA-DFT	Na_6[SOD]	1	*P*1			784.8	*C*2/*c* (No. 15)	
LDA-DFT	Na_6[SOD]	1	*P*1			745.8	*C*2/*c* (No. 15)	

[a] Procedures 1−4 are molecular mechanics results. The MM4 model is identical to MM2, and is included for a discussion about force field modeling techniques. MM3 produced the most realistic results, and is the model by which we will conduct hydration studies.

Table 4. Experimental Lattice Parameters for Na_6[SOD] Sodalite Compared to the MM, MD, and DFT Results of This Study, as Well as the DFT Results of Shannon et al.[16]

UCV (Å^3)	Δ (%)	*a* (Å)	*b* (Å)	*c* (Å)	α (deg)	*β* (deg)	*γ* (deg)	methodology	ref
759.0		9.122	9.122	9.122	90.00	90.00	90.00	P-XRD, RR (675 K)	33
757.1		9.114	9.114	9.114	89.78	89.78	89.78	S-XRD, rhombo-LBP	45
758.9		9.113	9.112	9.140	90.00	90.00	90.44	S-XRD, mono-LBP	45
758.8		9.113	9.111	9.139	90.00	89.98	90.43	S-XRD, tri-LBP	45
757.4		9.072	9.143	9.132	90.00	90.00	90.00	ortho-LBP	45
758.3		experimental average							
754.7	−0.5	9.107	9.107	9.107	91.34	91.34	91.34	MM1 (P)	this study
759.7	0.2	9.132	9.132	9.132	92.23	92.23	92.23	MM2 (P)	this study
748.0	−1.3	9.229	8.788	9.229	91.32	89.05	91.32	MM3 (P)	this study
767.6	1.2	9.167	9.161	9.154	91.74	91.84	91.81	NPT-MD (P)	this study
784.8	3.5	9.282	9.109	9.283	90.48	89.44	90.49	GGA-DFT (P)	this study
745.8	−1.6	9.138	8.933	9.139	90.64	89.16	90.64	LDA-DFT (P)	this study
765.8	1.0	9.149	9.149	9.149	89.67	89.67	89.67	GGA-DFT (P)	16
1496.1		13.159	12.943	8.788	90.00	91.85	90.00	MM3 (SC)	this study
1514.9		12.829	12.930	9.132	90.00	90.01	90.00	MM3 (SC), mono-RR (*P*2/*c* (30))	this study
1518.6		12.943	12.840	9.137	90.00	90.00	90.00	S-XRD, ortho-LBP	45
1536.3		12.972	12.912	9.172	90.00	90.00	90.00	DFT, ortho (*Pcn*2 (30))	16

*P*1 symmetry during the initial $[SOD]^{6-}$ minimization. MM2, however, uses the CCP−CP relaxation constraints and MM3 uses the CP relaxation constraints. The UCVs differ by 3.9 Å^3 (815.1 and 811.2 Å^3, respectively) after the initial minimization. More significant, however, are the UCVs after the secondary Na_6[SOD] minimization: the final UCVs differ by 11.7 Å^3 (759.7 and 748.0 Å^3, respectively), nearly three times larger than after the initial minimization. Because the secondary Na_6[SOD] minimizations were conducted the same way in both cases (*P*1/CP), there is no operational bias during that stage. As was the case for MM4/MM3, we also obtain different energies and resulting space groups between the two procedures.

As the two previous examples illustrate differences that *can* result from different minimization conditions, it is also instructive to illustrate how different procedures can produce the *same* final structure. Compare, for example, the MM2 and MM4 procedures. The initial $[SOD]^{6-}$ minimizations differ with respect to both symmetry and relaxation constraints (*P*1/CCP−CP and $P\bar{4}3n$/CP), while the secondary Na_6[SOD] minimization is identical in both cases. In this example, we see the greatest disparity in UCVs after the initial minimization—20.4 Å^3 (811.2 and 831.6 Å^3, respectively). However, the final UCVs are both 759.7 Å^3, the final lattice energies are the same, and both possess the same supercell symmetry.

The model with the lowest final lattice energy (MM2) was originally chosen to be the representative Na_6[SOD] model, but after some detailed structural characterizations, which follow, MM3 was chosen as the best model. We carry the results of MM1, MM2, and MM3 through the entire paper, however, to illustrate the differences between the three models. The criteria by which to choose the final Na_6[SOD] [BD] model is a complicated issue, and total energy alone is not sufficient. A closer look at the structural details became necessary.

Structural Parameters. Comparing theoretical results to observed values is a standard methodology by which to validate simulation results. Experimental results from two Na_6[SOD] studies[33,45] are used to validate the simulation results of this study in Table 4. We first compare the MM, MD, and DFT UCVs to the experimental mean of 758.3 Å^3. The results are very good: the MM results (models MM1−3) range between −1.3% and 0.2%, the NPT-MD (isothermal−isobaric ensemble) result deviates by 1.2%, and the DFT deviations are −1.6% and 3.5%.

We next compare T−O bond lengths, and O−T−O and Al−O−Si bond angles in Table 5. The MM Si−O bond lengths are generally better than the MM Al−O values, with average deviations of 0.3% and 3.9%, respectively. This may be reflective of the fact that Si−O bonds are stronger than Al−O bonds. The DFT results for the same parameters are more consistent—1.9% and 1.2%, respectively. Overall, the DFT results are slightly better than those of MM, noting that the MM Si−O values are noticeably better than DFT, while the MM Al−O values are noticeably worse than those of DFT.

Looking finally at O−T−O and Al−O−Si bond angles, it is relevant to point out that both simulation techniques produce bimodal O−T−O distributions, consistent with experiment, and confirming the presence of

Table 5. Mean T−O Bond Lengths, and T−O−T and O−T−O Bond Angles for the Three MM and Two DFT Models Produced in This Study

ref	Si−O (Å)	Δ (%)	Al−O (Å)	Δ (%)	O−Si−O (°)	Δ (%)	O−Si−O (°)	Δ (%)	O−Al−O (°)	Δ (%)	O−Al−O (°)	Δ (%)
33, 47	1.585		1.711		107.40		113.70		108.30		111.90	
45	1.599		1.714		107.13		114.27		107.92		112.62	
experimental average	1.592		1.713		107.27		113.99		108.11		112.26	
MM1	1.596	0.2	1.778	3.8	105.21	−1.9	113.63	−0.3	104.71	−3.1	113.82	1.4
MM2	1.597	0.3	1.781	4.0	105.52	−1.6	113.33	−0.6	104.67	−3.2	113.85	1.4
MM3	1.597	0.3	1.780	3.9	105.98	−1.2	112.85	−1.0	105.12	−2.8	113.62	1.2
GGA-DFT	1.631	2.5	1.745	1.9	106.08	−1.1	112.84	−1.0	105.32	−2.6	113.54	1.1
LDA-DFT	1.613	1.3	1.723	0.6	106.32	−0.9	112.58	−1.2	105.49	−2.4	113.37	1.0

distorted tetrahedra. The MM O−Si−O bond angles deviate by −1.6% and −0.6%, while the O−Al−O bond angles deviate by −3.0% and 1.3%. The DFT deviations for the same quantities are −1.0%, −1.1%, −2.5%, and 1.1%. Though the deviations for both techniques are nearly comparable, the DFT results are more consistent.

Comparing O−Al−O bond angles, the MM and DFT deviations are −3.0%, 1.3%, −2.5%, and 1.1%, respectively. Both of the MM and DFT Al/O results are not as good as the Si/O quantities. If we consider the magnitudes of the deviations, noting that the directionality of the deviations is consistent for both sets of results, the average deviation is 2.2% for MM and 1.8% for DFT. As with the previous discussions, slight advantage goes to DFT, which is also slightly more consistent. Looking finally at the Al−O−Si bond-angles, the MM and DFT deviations are −5.6% and −2.9%, respectively.

Generally speaking, DFT is slightly more accurate and slightly more consistent than MM, as expected. Both techniques show less accuracy with Al than with Si, noting that MM Si−O bond lengths are noticeably better than the DFT results. Because we are interested ultimately in the dynamical properties of hydrated sodalite, in the presence of diffusing extraframework cations, MM offers advantages over DFT due to its reduced computational demand. The DFT results are used here to justify the MM results. The MM results reported here are slightly better than those normally reported for force field-based simulations, which average approximately ±3−5%.

Ring Structures. This study identifies two structurally distinct oxygen sites in Na_6[SOD]. We postulate that these structurally distinct O-sites have different energetics, and as a consequence, are responsible for the new ring structures proposed here. Shannon et al.[16] contend that "vacant ring avoidance" drives supercell formation in Na_6[SOD] (vacant ring avoidance means that no two ^{V}S6Rs share a common tetrahedral atom), for which we concur. We offer more specific information, however, as to why vacant ring avoidance is the primary reason for supercell formation.

The proposed ring structures are illustrated in Figure 6 (b). These structures are noticeably different from the conventional rings illustrated in Figure 4 (a). These structures can be explained in terms of the two different O-sites that comprise the rings. A detailed structural analysis of the rings indicates that there are two ^{I}O-sites and four ^{II}O-sites (Figure 5 (b and c)) in the ^{O}S6R. These two ^{I}O-sites are also found directly opposite one another in the ring. We find that the $Na^{+}-{}^{I}O$ bond lengths are 2.224 and 2.259 Å, while the $Na^{+}-{}^{II}O$ sites are 2.330, 2.536, 2.881, and 3.340 Å. The shorter

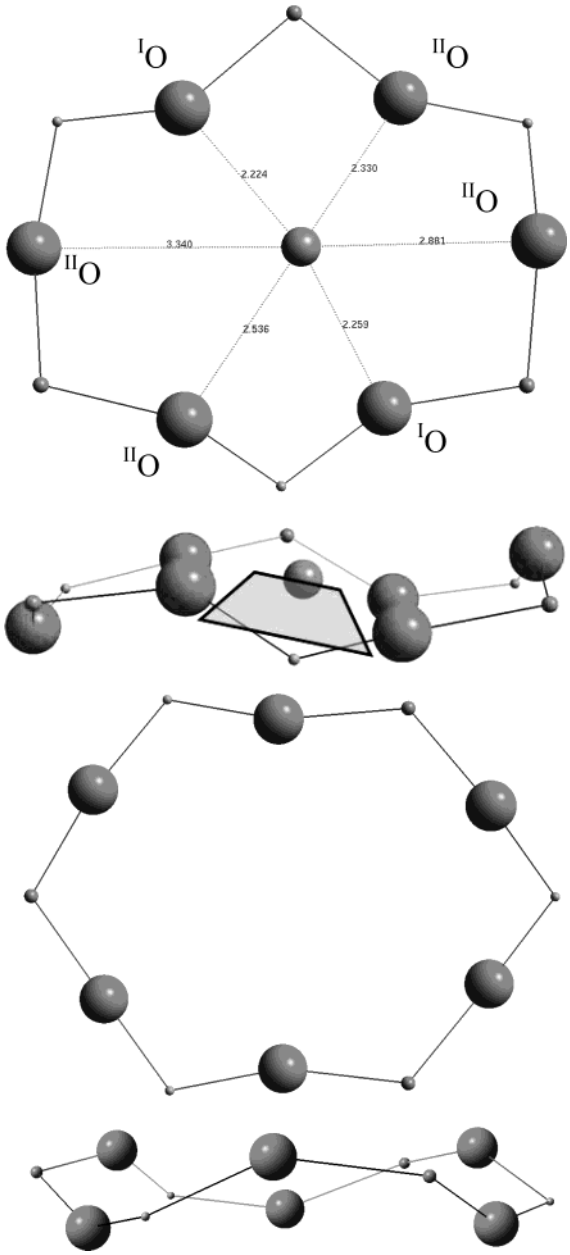

Figure 6. Proposed ring structures for Na_6[SOD]. All five final models (three MM and two DFT) produce the same basic ring structures. The structures can be explained in terms of two different oxygen types: two Type I (^{I}O), and four Type II (^{II}O) in the ^{O}S6R. The ^{I}O-sites are thought to be higher in energy, are found directly opposite one another in the ring, and are closer to the Na^{+} cation than any of the ^{II}O-sites. The lateral view of the ^{O}SR illustrates the planar nature of four O atoms in the ring and the central Na^{+} cation (see Figure 7).

Table 6. Bond Lengths and Bond Angles According to Oxygen Type

	bond lengths								bond angles											
	Si−^{I}O		Si−^{II}O		Al−^{I}O		Al−^{II}O		^{I}O−Si−^{I}O		^{II}O−Si−^{II}O		^{I}O−Al−^{I}O		^{II}O−Al−^{II}O		Al−^{I}O−Si		Al−^{II}O−Si	
	mean	SD	mean	SD	mean	SD	mean	SD	mean	SD	mean	SD	mean	SD	mean	SD	mean	SD	mean	SD
MM1	1.590	0.005	1.601	0.001	1.773	0.014	1.783	0.003	114.59	0.00	104.89	0.00	120.79	0.00	104.12	0.00	147.14	8.78	144.81	0.47
MM2	1.593	0.002	1.601	0.001	1.777	0.006	1.786	0.004	115.99	0.00	106.63	0.00	122.30	0.00	104.63	0.00	149.34	2.09	147.85	1.39
MM3	1.589	0.007	1.604	0.004	1.777	0.000	1.790	0.015	113.74	0.20	104.86	1.95	118.73	1.48	107.06	3.60	150.49	4.75	145.46	3.81
GGA-DFT	1.621	0.010	1.641	0.005	1.734	0.013	1.755	0.010	111.41	0.20	105.51	1.72	115.36	0.62	106.73	2.94	155.83	8.83	149.08	5.09
LDA-DFT	1.603	0.010	1.624	0.005	1.755	0.010	1.733	0.011	111.72	0.17	105.50	1.72	115.14	0.57	107.10	3.52	155.76	10.76	146.41	5.66

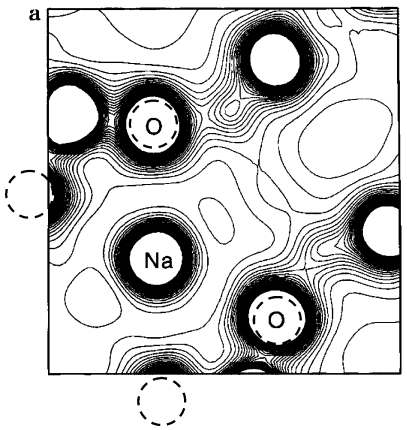

Figure 7. Maximum entropy method (MEM) charge density analysis of Na_6[SOD] at 675 K (from ref 48). The plot indicates that four framework O atoms and the central Na atom are coplanar, and that the four O atoms form a rectangular arrangement. The two remaining O atoms (not seen by the density plot) are not coplanar with Na. These results offer support for the simulation-based results presented in Figure 6. The dashed circles represent the locations of the four framework O atoms, and have been added to illustrate the atomic positions, especially for the two atoms outside the density plot.

interaction distances are attributed to higher energy O atoms. The ^{V}S6Rs are comprised entirely of ^{I}O atoms, and the ring is thought to form because of the more numerous and structurally important ^{O}S6Rs.

A reevaluation of some previously published experimental results supports the simulation-based conclusion that the S6Rs are distorted. Iversen et al.[48] carried out maximum entropy charge density analysis using synchrotron XRD data for three M_6[SOD] structures, where M = Na, Ag, and Tl. The results for Na are shown in Figure 7. The four framework O atoms and the central Na atom are coplanar, and the two remaining framework O atoms are not coplanar with the five atoms just mentioned, nor do they appear to be close to the plane, as zero charge density is attributed to these two O atoms. These results are consistent with the simulation-based results, suggesting a distorted S6R structure.

Bond lengths and bond angles can be used to compare the relative energetics of identical chemical species that reside in different chemical/structural environments.

Table 6 lists the average T−O bond lengths and T−O−T bond angles, according to oxygen type, for the five molecular models developed in this study. The T−^{I}O bond lengths are shorter than the T−^{II}O bond lengths for both Al and Si. These results are consistent with the idea that ^{I}O is higher in energy than ^{II}O. Unstrained aluminosilicate zeolites generally have T−O−T angles of approximately 144−45°,[49−51] as mentioned earlier. From Table 6, the T−^{I}O−T and T−^{II}O−T angles for MM3 are 150.5° and 145.5°, respectively. T−O−T angles that deviate from 144 to 45°—in either direction—are higher in energy. Thus, these results also support the hypothesis that Type I oxygens are higher in energy than Type II. This pattern exists for all five of the models developed in this study.

Supercell Formation. Supercell formation for Na_6[SOD] is based upon the loss of symmetry by the introduction of six sodium ions, rather than the usual eight expected for sodalite. Felsche and Luger[33] suggested that Na_6[SOD], at 675 K belongs to the $P\bar{4}3n$ space group, and report a R_{WP} value of 9.1% for this space group. This structural model assumes 75% occupancy of the 8*e* sites by the Na^+ ion. Refinements of models with higher-symmetry space groups ($Im3m$ and $I\bar{4}3m$) to allow for Si/Al disorder were not successful. They did not suggest supercell formation.

Shannon et al.[16] and Campbell et al.[45] are the first to suggest supercell formation in Na_6[SOD]. Shannon et al.,[16] using classical, force-field-based lattice energy minimizations and GGA-DFT, concluded that their C_{24} model is the most realistic (Table 4). Campbell et al.[45] used Le Bail profiles to fit room-temperature synchrotron XRD data to primitive rhombohedral, monoclinic, triclinic, and supercell orthorhombic crystal systems. The R_{WP} fitting parameters for these models are 10.39, 8.95, 8.93, and 8.59%, respectively. On the basis of these results, and a variety of XRD refinement results, they state that the supercell belongs to the *Pcn*2 space group (see previous comments). All of the molecular models developed in the current study support the supercell hypothesis.

It should be noted that Shannon et al. and ref 16 use both primitive cells and supercells to distribute the Na^+ ions. The same treatment discussed earlier concerning the [E], [FD], and [BD] arrangements is followed for the supercell, and the Na^+ ions are accordingly redistributed. In the supercell case, there are sixteen S6Rs in which to distribute 12 cations, producing 88 unique configurations. They then consider six low energy models in greater detail with GGA-DFT optimizations. We only consider the primitive cell by which to distribute the sodium ions.

All five of the models developed here support supercell formation. The existence of these supercells, as well as the specific space groups for each model, was determined using the Cerius2 space group module with

(48) Iversen, B. B.; Latturner, S.; Stucky, G. *Chem. Mater.* **1999**, *11* (10), 2912−2918.

(49) Megaw, H. D. *Crystal Structures: a Working Approach*; Studies in Physics and Chemistry, No. 10; Saunders: Philadelphia, PA, 1973.

(50) Depmeier, W. *Acta Crystallogr., Sect. B: Struct. Sci.* **1985**, *B41* (2), 101−108.

(51) Taylor, D.; Henderson, C. M. B. *Phys. Chem. Miner.* **1978**, *2* (4), 325−336.

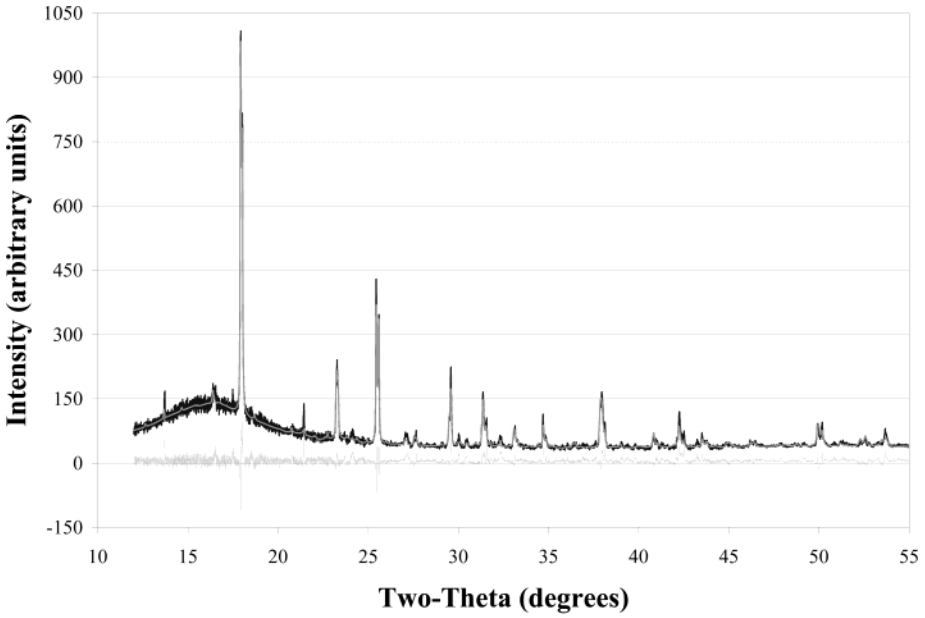

Figure 8. Simulated MM3 synchrotron XRD pattern compared to the room-temperature data of Campbell et al.[45] (major peak at ~10 degrees ignored due to complications with the refinements).

spatial tolerances of 0.1 Å: three (MM3 and both DFT models) are found to have *C*2/*c* monoclinic symmetry (space group No. 15), one (MM1) has *R*3*c* (space group No. 161) symmetry, and one (MM2) has $R\bar{3}$ (space group No. 148) symmetry (Table 3). We note here that the MM3 model has the same symmetry as both of the DFT models, which is taken as additional support for the MM3 model.

XRD Analyses. The various models were tested against Campbell et al.'s [ref 45, No. 268] room-temperature synchrotron-based XRD pattern ($\lambda = 1.1628$ Å) using the Rietveld and Le Bail methods[52] using the program FULLPROF2000.[53]

The Le Bail method (LBM) is a whole pattern profile refinement technique derived from the Rietveld method. In the LBM, as in the Rietveld method, the position of the diffraction peaks is a function of the cell parameters, that are usually refined; the intensities of the peaks, on the other hand, are not a function of a structural model but are iteratively estimated in order to obtain the best possible agreement between the calculated and observed patterns. The Le Bail method can therefore be applied without a full knowledge of the structure (that is, the atomic coordinates are not used). This method is therefore very powerful for assessing the adequacy of a proposed unit cell, checking the extinction laws and determining a space group, refining cell parameters in case of severe peak overlap, extracting peak intensities for subsequent structure solution, and obtaining good starting profile parameters for a Rietveld refinement. The LBM can be credited for the recent expansion of the field of ab initio structure solution from powder diffraction data.

It must be noted that the agreement factors obtained for a Le Bail refinement are always better than those of the corresponding Rietveld refinement because the peak intensities are not constrained by the structure but allowed to vary freely. Furthermore, the agreement indices used represent only a global measure of the quality of the fit and of the proposed models. For example, a better fit for some very weak superstructure peaks will only marginally contribute to the overall agreement factor, but can be crucial in discriminating between different models.

Although the unit cell volumes obtained from the various Na_6[SOD] sodalite structures derived from the molecular modeling techniques are very similar to observed values, the metric of the various unit cells departs too strongly from the original cubic one and leads to peak splittings more severe than those observed. Those starting cell parameters were first refined with strong damping factors and slowly converged to the more isometric values reported in Table 4. The various profile parameters describing the width and shape of the diffraction peaks, using a pseudo-Voigt profile and the usual parabolic Cagglioti function,[53] were subsequently freed. Those refined cell and profile parameters were then used to perform a pseudo-Rietveld refinement for the triclinic and monoclinic models in order to assess the reliability of the proposed structural models. The optimized atomic coordinates were then used to calculate the intensities of the diffraction peaks but were not varied; their values were kept fixed during the refinement. Reasonable temperature factors were assigned to the various atom types and only an overall temperature factor was refined, together with the lattice constants and cell parameters. This constrained refinement method gives a better estimation of the overall quality of the models than the Le Bail method alone because the atomic coordinates are used to constrain the intensities.

The agreement indices (Table 7) show that the Le Bail fit with the monoclinic cell is better than that with the triclinic one. The splitting of the peaks is not better explained with the triclinic cell which has more degrees

(52) Le Bail, A.; Duroy, H.; Fourquet, J. L. *Mater. Res. Bull.* **1988**, *23* (3), 447−452.

(53) Rodriguez-Carvajal, J. *FULLPROF: A Program for Rietveld Refinement and Pattern Matching Analysis*. In *Abstracts of the Satellite Meeting on Powder Diffraction of the XV Congress of the IUC;* Toulouse, France, 1990.

Table 7. MM3 Rietveld Refinement Results

refinement	R_P	R_{WP}
MM3/*P*2/*c*/RR	7.91	10.50
MM3/*P*2/*c*/LB	6.18	7.92
*Pcn*2/RR [*16*]		10.57
ortho/LB [*45*]	7.03	8.59

of freedom, and the cell parameters are, as expected, very strongly correlated with each other. This indicates that the triclinic description is probably not adequate. An analysis of the refined triclinic cell[54,55] shows that the cell metric is of the monoclinic system and corresponds to a C-centered supercell with a volume twice as large, with $a' \approx a\sqrt{2}$, $b' \approx a\sqrt{2}$, $c' \approx a$, and $\beta \approx 90°$, a being the cell parameter of the parent cubic phase. The C-centering detected is inherent to this type of cell distortion and is not necessarily the most correct centering mode.

The LeBail refinements indicate several weak but significant peaks or clusters of peaks that could not be indexed by the C-centered supercell (space group *C*2/*c*), nor by the original triclinic one. However, these peaks could be indexed by a primitive supercell with the same lattice constants, using the space groups *P*2/*c* or *P*21/*c*, which are both subgroups of *C*2/*c*. The agreement factor R_P of the LeBail fit decreases markedly from 6.76 to 6.18% when the C-centering is dropped. Although the β angle refines to 90.030(9)°, a primitive orthorhombic cell (fixing β to 90°) gives a significantly poorer fit with $R_P = 6.34\%$. The primitive monoclinic cell appears therefore to be the most satisfactory model for Na_6[SOD] (Figure 8).

Cage Structure. The primary structural consequence of supercell formation is the creation of two unique β-cages that alternate positions in a three-dimensional "checkerboard" type of pattern. Recall that the ideal sodalite framework is constructed from octahedrally coordinated β-cages (Figure 2). When considering a sodalite framework that incorporates two differently sized β-cages in equal proportions, however, a more convenient way to conceptualize the framework is to envision two separate, yet interlinked, *cubic* arrays of β-cages, where the β-cages are connected via their S4Rs. This can be envisioned by considering the light gray β-cages in Figure 2 and then extrapolating the central, black β-cage sub-lattice similarly. Every β-cage is connected to a total of 14 distinct β-cages: eight β-cages through the S6Rs and six through the S4Rs.

A simple analogy by which to better understand this structural description is to consider the CsCl structure: every Cl^- ion has eight nearest neighbors in the ⟨111⟩ directions, all of which are Cs^+. Likewise, every Cl^- has eight nearest neighbors, all of which are Cl^-. With respect to the exclusive consideration of each chemical species unto themselves, however, the Cs^+ and Cl^- ions form cubic sublattices (⟨001⟩ directions). In this simple analogy, one β-cage sublattice would correspond to the Cs^+ ion sublattice, and the second β-cage sublattice would correspond to the Cl^- ion sublattice.

The two arrays of β-cages are not independent structural elements, of course, and cannot be actually separated into two separate sublattices. The S6Rs are single

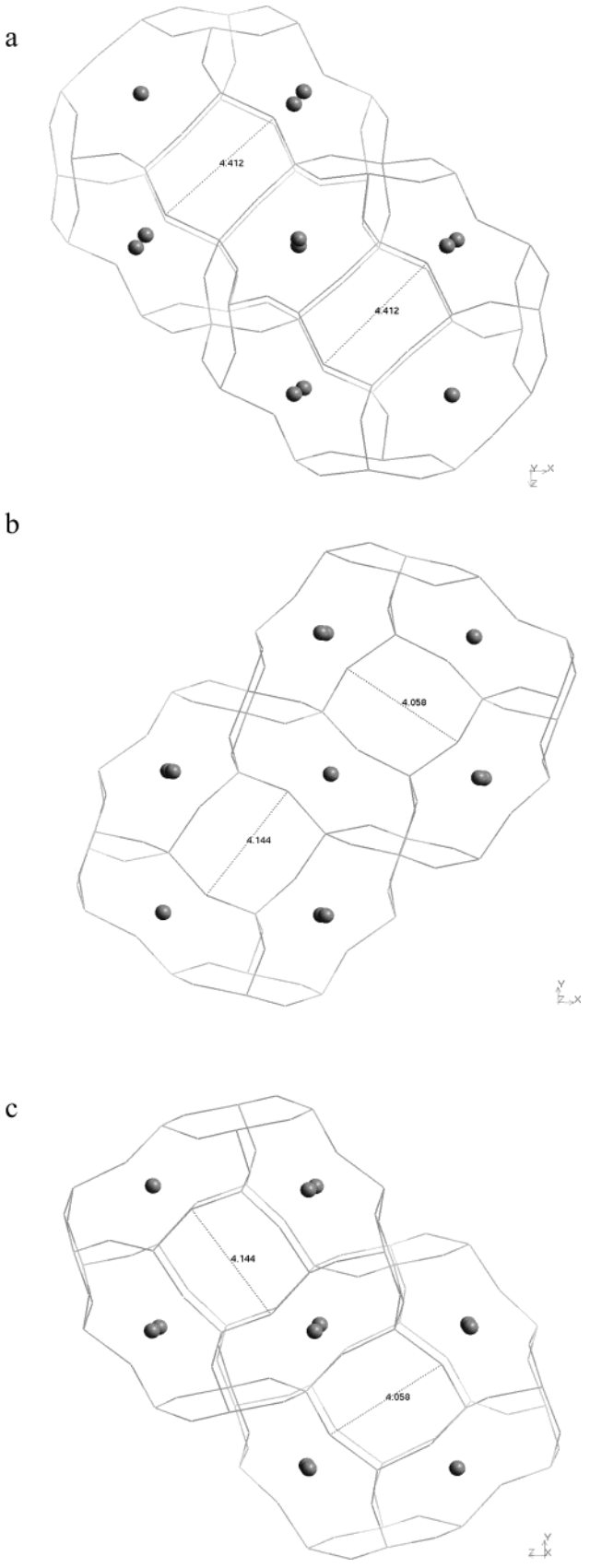

Figure 9. S4R O−O distances (longest) dimensions in Na_6[SOD] (MM3). (a) Looking at the two cages from the [010] direction; in this case, the two S4Rs are equivalent. (b) Looking at the two cages from the [001] direction; the two S4Rs are not the same. (c) Looking at the two cages from the [100] direction; in this case, the two cages have "switched" the values seen in (b).

(54) Spek, A. L. *J. Appl. Crystallogr.* **1988**, *21* (5), 578−579.
(55) Le Page, Y. *J. Appl. Crystallogr.* **1987**, *20* (3), 264−269.

rings, not double rings, and the features are common to both sublattices: any change in the dimensions of the S6Rs effect both sublattices equally. However, this is not true of the S4Rs. The S4Rs are unique to one of the two sublattices, but not both. The S6Rs might therefore be called *inter*-lattice structural elements, and the S4Rs might be called *intra*-lattice structural elements (with respect to the cubic sublattices). Thus, examining S4Rs will provide more direct information about potentially asymmetric cage structures than would examining the S6Rs.

The distances between opposing O atoms in the S4Rs (two pairs per S4R) were measured systematically from cage to cage. To facilitate this analysis the following steps were taken: (1) a $3 \times 3 \times 3$ supercell was constructed from the original supercell, (2) the model was converted to a superlattice, and (3) the model was reduced to a nonperiodic superstructure. The remaining "grain" of material was then whittled down to contain a series of cages, as viewed from the three directions of interest. In the original supercell, the S4Rs align in the ⟨001⟩ directions. For convenience, we align the S4Rs in Figure 9 in the ⟨001⟩ directions. The supercell is related to the primitive cell as $a' = a - c$, $b' = -a - c$, $c' = b$, which produces a transformation matrix with a discriminant of two. Every S4R has two pairs of opposing atoms, and one pair was always found to be longer than the other. For convenience, only the longest O−O distances are reported and discussed.

The S4Rs were not found to be symmetric from sublattice to sublattice in two of the three directions specified (Figure 9). Whereas the S4Rs are the same for both sublattices in the ⟨001⟩ direction (Figure 9(a)), the S4Rs in the *y* (Figure 9(b)) and *z* (Figure 9(c)) directions are not the same size. Looking more closely, it becomes apparent that the S4Rs switch positions in the *y* and *z* directions from one sublattice to the other. If the first β-cage has dimensions $x_1y_1z_1$, the second β-cage has dimensions $z_1y_1x_1$. Thus, while the overall dimensions of the two cages are identical, the two cages are enantiomers.

Table 8 lists the longest opposing O−O distances in the S4Rs for the five models developed in this study. The MM1 results do not suggest the presence of two β-cages. Although it initially appears that there are two differently sized cages in MM2, this arrangement does not appear realistic because a complete reversal in O−O distances—the $^{I}O-^{I}O$ distances are the longest in Cage 1 and the shortest in Cage 2—is observed. While this trend, in and of itself, may not rule out the suitability of MM2, when we consider MM3 and the two DFT results, the MM3 results appear to be most realistic. Both DFT models and MM3 clearly suggest (a) three different S4Rs in one uniquely dimensioned cage, and (b) a clear rotation of the β-cage about the *y*-axis. Figure 9 illustrates the pattern in all three directions. For this reason and others, MM3 was chosen to be the most realistic model to represent the Na_6[SOD] structure and to provide a base for future hydration studies.

Table 8. O−O Distances *Across* the S4Rs in Na_6[SOD][a]

	Cage 1		Cage 2	
direction	$^{I}O-^{I}O$	$^{II}O-^{II}O$	$^{I}O-^{I}O$	$^{II}O-^{II}O$
		MM1		
[100]	3.80	3.78	3.80	3.78
[010]	3.80	3.78	3.80	3.78
[001]	3.80	3.78	3.80	3.78
		MM2		
[100]	4.09	3.75	3.89	4.00
[010]	4.09	3.75	3.89	4.00
[001]	4.09	3.75	3.89	4.00
		MM3		
[100]	*4.14*	*3.73*	3.94	4.06
[010]	3.31	4.41	3.31	4.41
[001]	3.94	4.06	*4.14*	*3.73*
		GGA-DFT		
[100]	*4.27*	*3.68*	3.77	4.22
[010]	3.56	4.33	3.55	4.34
[001]	3.76	4.23	*4.28*	*3.67*
		LDA-DFT		
[100]	*4.29*	*3.55*	3.63	4.25
[010]	3.37	4.37	3.36	4.37
[001]	3.62	4.26	*4.30*	*3.54*
		Shannon C24		
[100]	*3.80*	*3.80*	3.86	3.86
[010]	3.90	3.90	*3.80*	*3.80*
[001]	3.96	3.61	3.67	4.13

[a] Cage 1 is always the fully constructed β-cage in the primitive cells, and Cage 2 is a fractional cage in the eight corners. All ⟨001⟩ directions are with respect to the primitive cells. The presence of one or two unique β-cages can be identified by examining the S4Rs. MM1 only has one unique β-cage. MM2 has two different β-cages. MM3 and both DFT results suggest two unique cages that have the same overall size but different orientations. If the first cage has dimensions *xyz*, the second cage has dimensions *yxz*; in other words, they are enantiomers. The slight asymmetry (0.01 Å) observed in the DFT results is neither unusual nor unexpected.

Conclusion

Energy minimizations, molecular dynamics, and density functional theory simulations of anhydrous $Na_6[Si_6Al_6O_{24}]$ sodalite have been performed as part of an Environmental Management and Science Program (EMSP) project sponsored by the U.S. Department of Energy (DOE) to address the spontaneous precipitation of sodalite and cancrinite phases in nuclear-waste treatment and disposal facilities. All of the simulation results from this study suggest that anhydrous $Na_6[Si_6Al_6O_{24}]$ sodalite forms a supercell with twice the unit volume as the primitive cell, in agreement with recent simulation and experimental results.[16,45] Whereas the recent reports suggest *Pcn*2 and orthorhombic symmetries, our refinements, using the same experimental synchrotron X-ray powder diffraction data, produce better Le Bail and Rietveld refinement parameters for the *P*2/*c* space group. We further propose a new S6R structure for $Na_6[Si_6Al_6O_{24}]$ sodalite, a result that can be explained in terms of two structurally and energetically distinct oxygen sites. This structural result offers more specific evidence to support of the recent hypothesis that "vacant ring avoidance" drives supercell formation. The primary structural result of the new S6R is the formation of two alternating, enantiomeric β-cages. The XYZ and YXZ nature of the two enantiomeric β-cages, and their uniqueness in two of the three dimensions, explains the volume-doubled unit cell, as required for an accurate description of the symmetry.

Acknowledgment. We thank an anonymous referee for the comments provided. Louise Criscenti and May Nyman also provided suggestions that contributed to

an improved manuscript. We are appreciative of funding provided by the U.S. Department of Energy, both the Office of Basic Energy Sciences, Geosciences Research, and the Environmental Management and Science Program (DE-FG07-01ER63298). Sandia is a multiprogram laboratory operated by Sandia Corporation, a Lockheed Martin company, for the U.S. Department of Energy under contract DE-AD04-94AL85000.

CM0352302